Role of Compliant Leg in the Flea-Inspired Jumping Mechanism

Gwang-Pil Jung, *Student Member, IEEE,* Ji-Suk Kim, Je-Sung Koh, *Student Member, IEEE,* Sun-Pil
Jung and Kyu-Jin Cho, *Member, IEEE*

Abstract—Jumping locomotion has been widely employed in milliscale mobile robots to help overcome their size limitations by extending their range and enabling them to overcome obstacles. During jumping, the robot's legs experience acceleration that is up to an order of magnitude greater than the gravitational acceleration. This large force results in bending of the jumping legs. In this paper, we study how the bending of the leg affects the jumping performance of a flea-inspired jumping robot. To judge the effect of the leg compliance, the amount of energy lost during jumping is determined by examining the ratio of kinetic energy to input energy, which we define as the mechanical efficiency. The bending leg is dynamically modeled using a pseudo-rigid-body model in order to precisely analyze the energy transfer. Jumping experiments are performed for five different legs, each with a different stiffness. Shape memory polymer rivets, which are lightweight and compact, were used to easily switch out the legs. The mechanical efficiency of the robot with appropriately chosen leg compliance was 41.27% compared with 36.93% for the rigid case and 21.51% for the much more compliant case. The results show that optimizing the compliance of a jumping leg can improve the performance of a jumping robot.

I. INTRODUCTION

Jumping locomotion has been widely employed in small-scale mobile robots to enable them to overcome large obstacles and distances. To achieve high jumping height, a variety of mechanisms are employed, such as an escapement mechanism using a cam or gear [4–7], snap-through buckling [8], torque-reversal [1–3], one-way bearing [9], an inchworm motor [10] and chemical energy [11]. To maximize takeoff speed, more powerful actuators, large energy storages, and robust robot frames have been used. However, maximizing the jumping ability using bulk energy storage has limitations in terms of weight and structural integrity.

Jumping ability can also be improved by employing a more efficient jumping mechanism. Locomotion efficiency can be described by the cost of transport [12], defined as the kinetic energy divided by the product of the weight and moving distance. The cost of transport allows us to compare different types of locomotion. However, this measure does not account for losses during conversion of stored energy to kinetic energy. To quantify the efficiency of a mechanism
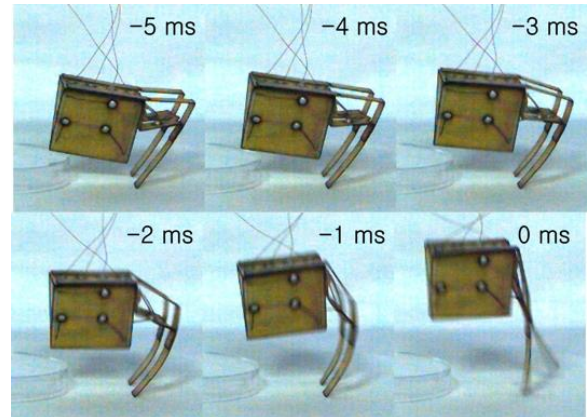
Fig. 1. Bending Leg in the Flea-inspired jumping mechanism [1]

itself, we define mechanical efficiency as the ratio of the kinetic energy to the input energy in the actuator.

Jumping robots operate by the following three-step process. First, energy storage is charged with energy. Second, the stored energy is released rapidly through transmission mechanisms such as four-bar or six-bar links and transferred to the relatively long jumping legs, chosen for power amplification. Finally, the force is transmitted to the ground and the robot takes off. Through this process, the initially stored energy is converted into five types of energy: rotational kinetic, translational kinetic, potential, vibrational, and residual energy, where residual energy is the unconverted part of the initially stored energy.

The energy flow of the jumping robot proceeds from energy storage to the transmission mechanism and finally to the legs. Among those three components, the bending of the jumping leg is most likely to influence the mechanical efficiency. The jumping robots experience an acceleration twelve times that of gravity during takeoff, which induces bending moments or compression that deform the jumping leg, as shown in Fig. 1.

In this paper, we study how the leg compliance affects mechanical efficiency. To precisely analyze the energy transfer during jumping, a dynamic model of the flea-inspired jumping mechanism is derived. In the model, the leg compliance is described as a torsional spring based on the pseudo-rigid-body model (PRBM) [13]. With the proposed dynamic model, the distribution of input energy at takeoff is analyzed. We experimentally verify the effect of leg compliance using five legs of different stiffnesses.
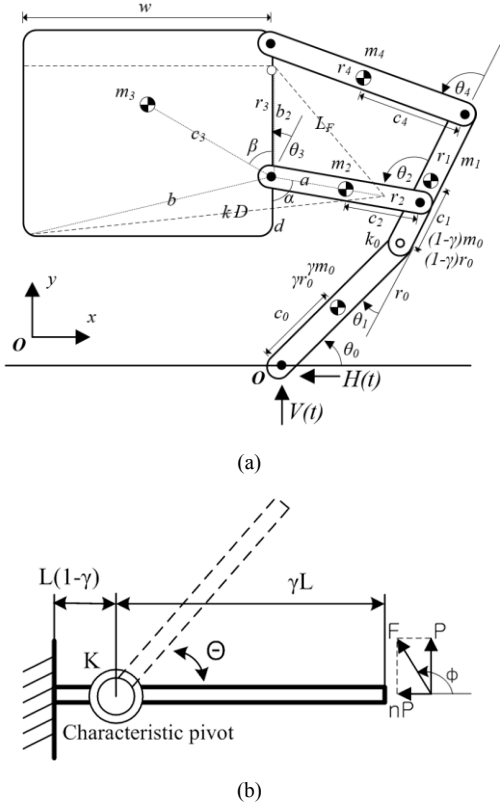
(a)

(b)

Fig. 2 (a) Schematic used for modeling and (b) the corresponding PRBM model of the compliant leg [12]. The origin is located at the point where the reaction forces are exerted.

II. COMPLIANT LEG ANALYSIS

To investigate how stored energy is transferred during jumping, the compliance of the jumping leg will be modeled. However, linear beam theory is difficult to apply to this case as the leg of the flea-inspired mechanism experiences large deflection when it takes off, as shown in Fig. 1. Also, for highly compliant legs, the extent of deflection further increases.

To analyze beams undergoing large deflection, the PRBM is used [13]. The PRBM provides a simple method to analyze the large-deflecting beam by replacing the beam with a flexural pivot and multiple rigid beams, depending on the loading condition.

A. Modeling of Leg Compliance

As previously stated, the compliant beam can be modeled differently depending on the loading condition. In this case, one end of the leg is fixed to a four-bar mechanism and the other is freely loaded; therefore, the jumping leg is regarded as a cantilevered segment with forces at the free end. As shown in Fig. 2, the compliant leg is modeled with one torsional spring and two rigid links.

Next, the location and the stiffness of the torsional spring are determined. The characteristic radius factor, γ, and the stiffness coefficient, K_θ, are determined for a particular loading condition with load direction, n, and maximum pseudo-rigid-body angle, Θ_{max}. Based on the reaction force curve presented in previous research [1], the parameters

TABLE III. PRBM PARAMETERS

Direction of reaction force, n	Characteristic radius factor, γ	Max. pseudo-rigid-body angle, Θmax (deg)	Stiffness coefficient, Kθ
2	0.8276	69	2.59707

indicating the loading condition of the reaction force are determined and are presented in Table 1. The stiffness of the torsional spring is given as $k = \gamma K_\theta EI/L$, where E is Young's modulus, I is the moment of inertia, and L is the length of the compliant leg.

B. Dynamics

The modified model consists of five rigid links and six rotational joints. To model the mechanism, five variables, θ_0, θ_1, θ_2, θ_3, and θ_4, are used to indicate the position, P_i, of each link.

$$\overrightarrow{P_0} = \begin{pmatrix} c_0 \cos\theta_0 \\ c_0 \sin\theta_0 \end{pmatrix} \tag{1}$$

$$\overrightarrow{P_1} = \begin{pmatrix} \gamma r_0 \cos\theta_0 + c_1 \cos(\theta_0 + \theta_1) \\ \gamma r_0 \sin\theta_0 + c_1 \sin(\theta_0 + \theta_1) \end{pmatrix} \tag{2}$$

$$\overrightarrow{P_2} = \begin{pmatrix} \gamma r_0 \cos\theta_0 + (1-\gamma)r_0 \cos(\theta_0 + \theta_1) \\ \quad + c_2 \cos(\theta_0 + \theta_1 + \theta_2) \\ \gamma r_0 \sin\theta_0 + (1-\gamma)r_0 \sin(\theta_0 + \theta_1) \\ \quad + c_2 \sin(\theta_0 + \theta_1 + \theta_2) \end{pmatrix} \tag{3}$$

$$\overrightarrow{P_3} = \begin{pmatrix} \gamma r_0 \cos\theta_0 + (1-\gamma)r_0 \cos(\theta_0 + \theta_1) \\ \quad + r_2 \cos(\theta_0 + \theta_1 + \theta_2) + c_3 \cos(\theta_0 + \theta_1 + \theta_3 + \beta) \\ \gamma r_0 \sin\theta_0 + (1-\gamma)r_0 \sin(\theta_0 + \theta_1) \\ \quad + r_2 \sin(\theta_0 + \theta_1 + \theta_2) + c_3 \sin(\theta_0 + \theta_1 + \theta_3 + \beta) \end{pmatrix} \tag{4}$$

$$\overrightarrow{P_4} = \begin{pmatrix} \gamma r_0 \cos\theta_0 + ((1-\gamma)r_0 + r_1)\cos(\theta_0 + \theta_1) \\ \quad + c_4 \cos(\theta_0 + \theta_1 + \theta_4) \\ \gamma r_0 \sin\theta_0 + ((1-\gamma)r_0 + r_1)\sin(\theta_0 + \theta_1) \\ \quad + c_4 \sin(\theta_0 + \theta_1 + \theta_4) \end{pmatrix}, \tag{5}$$

where r_i is the length of each link, c_i is the distance between the center of mass of each link and the adjacent joint, and β is the angle between r_3 and c_3.

The entire mechanism has three degrees of freedom, and the four-bar mechanism has the following kinematic constraints:

$$r_1 + r_4 \cos\theta_3 = r_2 \cos\theta_2 + r_3 \cos\theta_4 \tag{6}$$

$$r_4 \sin\theta_3 = r_2 \sin\theta_2 + r_3 \sin\theta_4 . \tag{7}$$

With the positions and the kinematic constraints, the dynamics of the jumping are numerically determined by a Lagrange formulation. The initial conditions of the jumping mechanism are set as follows:

$$\theta_0 = 57° \tag{8}$$

$$\theta_1 = 0° \tag{9}$$

$$\theta_2 = 126.05° \tag{10}$$

TABLE IV.   Leg Dimensions of Compliant Legs

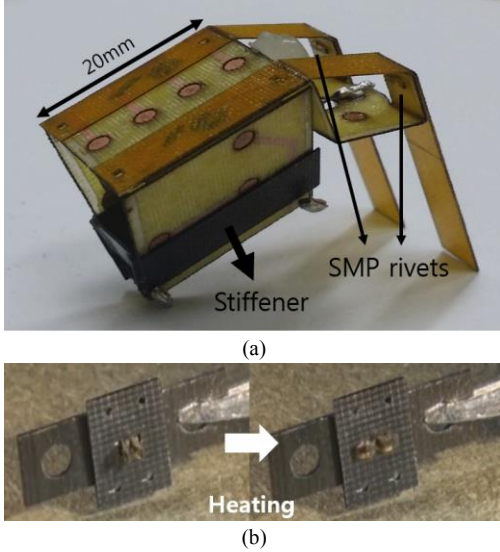| Sample No.	Material	Number of layers	Thickness (mm)	Width (mm)	Length (mm)	Young's Modulus (Gpa)	Weight (g)	Bending stiffness (Nm/rad)
1	CFRP	6	0.58	6	19.5	31.3751	0.1	0.3373
2	GFRP	21	0.64	6	19.5	7.3058	0.1	0.1288
3	GFRP	21	0.64	2	19.5	7.3312	0.1	0.0434
4	GFRP	10	0.39	6	19.5	7.3547	0.1	0.0248
5	GFRP	4	0.27	6	19.5	7.3242	0.1	0.0078

(a)

(b)

Fig. 3 (a) The Flea-inspired jumping mechanism assembled with SMP rivet fasteners [15]. The leg in this figure is sample no. 4. The stiffener is the 6 layers of cured CFRP to reinforce the body. (b) The operation of SMP rivet fastener [16]

where θ_0 is the angle between the jumping leg and the ground, θ_1 is the initial bending angle of the jumping leg, and θ_2 is the angle that determines the orientation of the four-bar transmission. Note that the value of θ_2 is set to simulate the state just before jumping.

Takeoff of the jumping mechanism occurs when the vertical reaction force, $V(t)$, is zero. The x and y components of the force exerted on the robot are given by

$$m_{robot} a_{robot,x} = \sum_{i=0}^{4} m_i a_{i,x}(t) = -H(t) \tag{11}$$

$$m_{robot} a_{robot,y} = \sum_{i=0}^{4} m_i a_{i,y}(t) = V(t) - \sum_{i=0}^{4} m_i g, \tag{12}$$

where m_{robot} is the total mass of the robot, a_{robot} is the acceleration of the robot's center of mass, a_i is the acceleration of each link, and H is the horizontal reaction force on the ground. The translational and angular velocities during takeoff are given by Eqs. (13) and (14), respectively.

$$m_{robot} v_{robot} = \sum_{i=0}^{4} m_i v_{i,f} \tag{13}$$

$$m_{robot} w_{robot} = \sum_{i=0}^{4} m_i w_{i,f} , \tag{14}$$

where v_{robot} is the velocity of the robot's center of mass and w_{robot} is the angular velocity of the robot. $v_{i,f}$ and $w_{i,f}$ are the translational velocity and angular velocity of each link just before takeoff.

III. Assembly of the Jumping Leg

Five jumping legs of different stiffnesses are prepared. Table 2 lists the material, dimensions, Young's modulus, and bending stiffness of each leg. Young's modulus is measured using the three-point bending experiment. The bending stiffness, k, is calculated using these measurements of E in the relation, $k = \gamma K_\theta EI/L$.

The jumping legs are made of glass fiber reinforced prepreg (GFRP) and carbon fiber reinforced prepreg (CFRP). GFRP is used for the highly compliant legs, and the stiffness is modified by adjusting the number of layers. The rigid leg is fabricated using six layers of CFRP, as listed in Table 2, which resulted in a high bending stiffness. Additional weights, tiny metallic bars, are attached to the center of the bending leg to standardize the weights of the jumping legs, which differ owing to material choice and the number of layers.

In the jumping experiments, the same flea body is used across all trials to maintain the same initial stored energy in the extensor. To easily switch the legs and minimize damage, shape memory polymer (SMP) rivet fasteners [15] are employed, as shown in Fig. 3 (a). SMP is well known for shape recovery and modulus alteration, which is induced by temperature changes as shown in Fig. 3 (b). With these properties, SMP rivet fasteners can be reversibly used and can achieve a high disengagement force of up to 7 N [15] while weighing only 0.003 g each. The SMP rivet fastener is designed as a simple I-beam shape and is installed through a hole inside the four-bar transmission mechanism, as shown in Fig. 3 (a).

A shape memory alloy (SMA) coil spring actuator is used as the extensor. The extensor has ten active coils and a spring coefficient of 300 N/m in the austenite phase. The body of the mechanism is reinforced with six layers of CFRP, as shown in Fig. 3, in order to prevent deformations by repeated actuation.

IV. Results

This study was initiated to investigate how compliant legs affect jumping performance. To examine the influence of the compliant leg, several jumping experiments were conducted by varying the bending stiffness of the jumping legs.

Determining the mechanical efficiency of the mechanism at takeoff via jumping experiments is problematic, even with the use of a high-speed camera. The extensor cannot be visualized since it is located inside the body, making it difficult to determine the remaining extensor energy at takeoff. To calculate the precise mechanical efficiency, we analyze the energy distribution with the proposed dynamic model after validation.
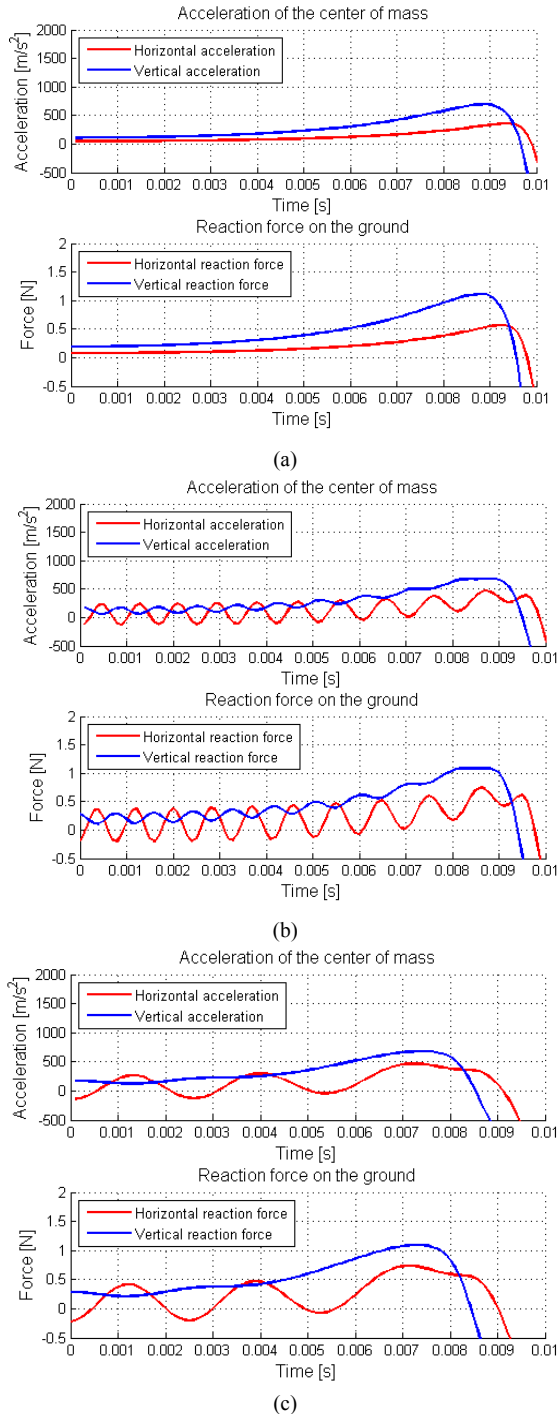

(a)

(b)

(c)

Fig. 4 Acceleration and reaction force on the ground (modeling data). (a) Model with rigid leg (b) Stiffness of 0.6746 Nm/rad (c) Stiffness of 0.0869 Nm/rad

TABLE V. TAKE-OFF ANGLE

Leg stiffness (Nm/rad)	Takeoff angle (deg)	
	Simulation	Experiment
Rigid	64.6	-
0.6746	66.0	71
0.2576	65.4	77
0.0869	64.0	76
0.0496	64.1	75
0.0156	69.1	82

A. Jumping Experiments

The jumping experiment is implemented using five legs of different bending stiffnesses, as described in Table 2. Three jumps are recorded for each of the five legs using a high speed camera with a frame rate of 5,000 fps. Data is analyzed with a ProAnalyst—a video analyzing tool—and is filtered using a first order low pass filter with a cutoff frequency of 270 Hz. Through this process, the takeoff time, takeoff angle, velocity, and leg bending angle are calculated.

B. Model Validation

Fig. 4 shows the acceleration of the robot and the reaction force on the ground. Fig. 4 (a) shows results of the rigid leg model used for the previous flea-inspired jumping mechanism [1]. Figs. 4 (b) and 4 (c) show results of the legs with stiffnesses of 0.6746 N/rad and 0.0869 Nm/rad, respectively. The major difference between the rigid and the compliant leg models is the vibration of the jumping leg. With this model, the efficiency of energy conversion from input energy to leg vibrational energy can be calculated. As shown in Fig. 4, the frequency of the leg vibration during jumping increases with leg stiffness, following the natural frequency.

Fig. 5 shows the takeoff velocity of the model. As the stiffness increases, the data from the compliant model converges to that of rigid model. Simulated and experimental values agree well for data in the y direction. However, velocity data in the x direction show a mismatch between
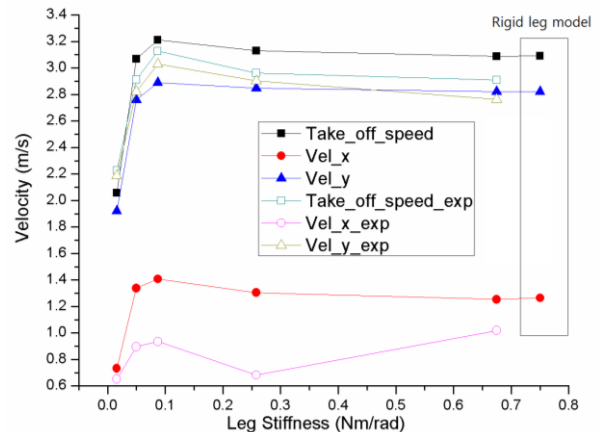

Fig. 5 Takeoff velocity. The data in the box at the right side is from the rigid leg model.

Fig. 7 Energy distribution at takeoff. The graph is plotted with the modeling data.

Fig. 8 Mechanical efficiency of the jumping mechanism with various leg stiffness. Mechanical efficiency of the experiment is determined using the measured kinetic energy and it was divided by the same input energy calculated from the simulation.
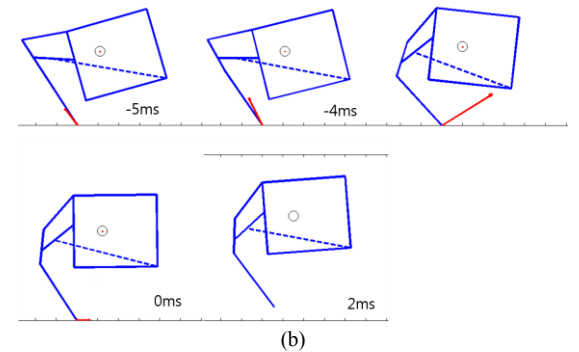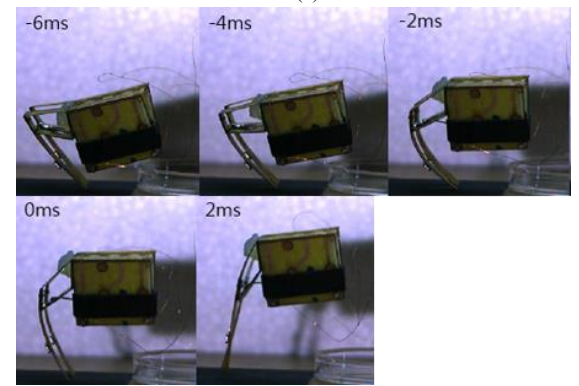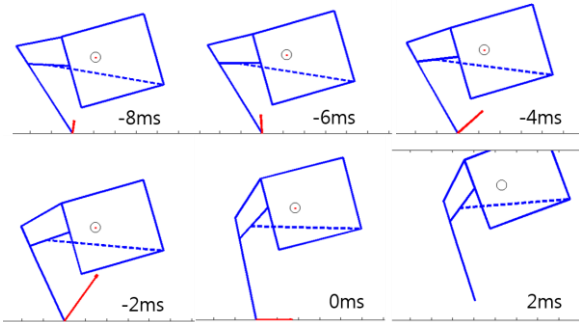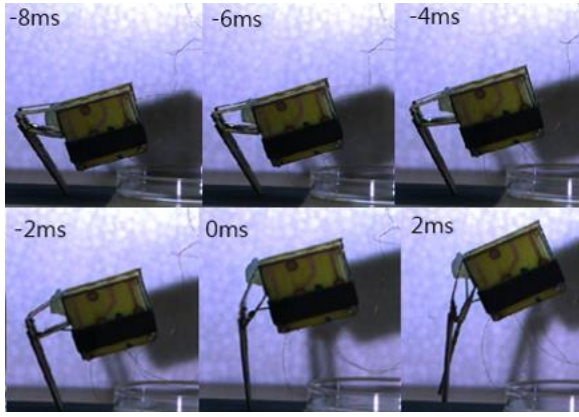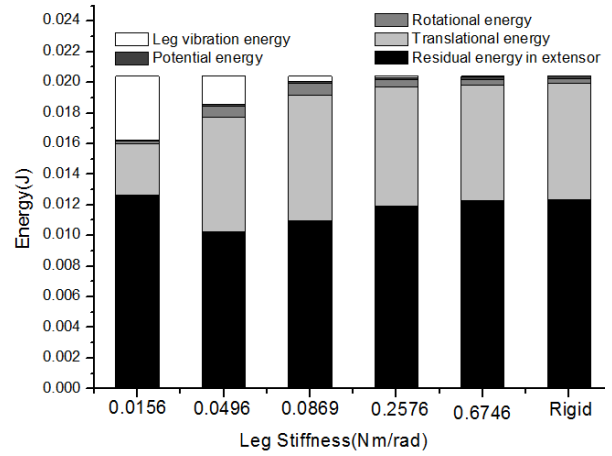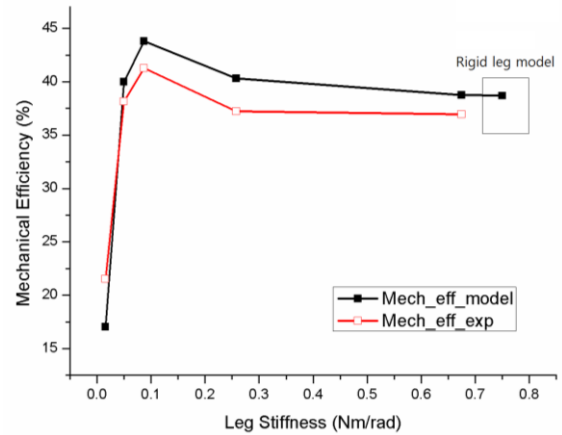
(a)

(b)

Fig. 6 The jumping sequence of the Flea-inspired mechanism and its model visualization. Leg stiffness of (a) 0.6746 Nm/rad (b) 0.0156 Nm/rad. Red line indicates the reaction force vector and the circle inside the body is the center of mass. Note that the velocity at take-off is reflected in the model visualization after take-off, maintaining robot configuration.

simulation and experiment, which is likely due to slippage at takeoff. The slippage occurs when the vertical reaction force rapidly drops to zero while the horizontal reaction force is nonzero. Therefore, slippage occurs when the base does not have a high enough coefficient of friction.

Because of slippage in the x direction, the body slightly moves backward and the takeoff angle increases, as indicated in Table 5. The takeoff angle difference is also observed in Fig. 6, which illustrates jumping using both experimental pictures and model visualization. The takeoff angle of the experimental case is steeper than that of the model.

C. Energy Distribution at Take-off

To investigate the mechanical efficiency of the jumping mechanism, energy distribution at takeoff is calculated based on the simulation. When the mechanism jumps, the initial input energy in the extensor is transferred to translational kinetic energy, rotational kinetic energy, and vibrational energy of the leg. Also, there is residual extensor energy, which is the unconverted part of the initially stored energy.

The energy distribution at takeoff is shown in Fig. 7. Leg vibrational energy and residual extensor energy, both of which contribute to inefficiency, vary with leg stiffness. As shown in Fig. 6 (b), the compliant leg bends at takeoff, suggesting that leg vibrational energy will increase with leg compliance. This phenomenon is illustrated in Fig. 7.

The residual energy exhibits somewhat different behavior. The amount of the residual energy decreases as the stiffness decreases down to 0.0496 Nm/rad. Over this range, the initially stored energy is increasingly converted to kinetic and vibrational energy as the leg compliance increases. In the highly compliant case, however, the residual energy itself increases, suggesting that the mechanism takes off before completing the energy transfer and the robot prematurely leaves the ground [14].

Based on the above energy analysis, the mechanical efficiency is calculated. As shown in Fig. 8, the leg with a stiffness of 0.0869 Nm/rad shows the maximum mechanical efficiency at 43.79% (41.27% experimental).

V. CONCLUSION

In this paper, we studied how leg compliance affects mechanical efficiency. Based on simulation and experimental results, an optimal range of leg compliance that can increase jumping performance was determined. Using the PRBM model, we precisely analyzed the transfer of input energy to minimize the vibrational energy of the jumping leg while maximizing the kinetic energy released from the energy stored in the actuator spring. The effect of the compliant leg was confirmed by jumping experiments using legs of varying stiffnesses.

In future studies, the jumping dynamics need to be optimized according to takeoff angle in addition to leg stiffness. When the takeoff angle changes, the mass distribution of the robot varies and the optimal leg compliance may vary as well. Additionally, the slippage problem must be resolved in order to obtain more precise experimental results. Finally, symmetric jumping mechanisms [2,3] should be implemented to eliminate rotation of the robot body. This rotation make analysis difficult and usually occurs owing to reaction forces not passing through the center of mass.

REFERENCES

[1] M. Noh, S. Kim, S. An, J. Koh and K. Cho, "Flea-Inspired Catapult Mechanism for Miniature Jumping Robots", *Robotics, IEEE Transactions on (TRO)*, vol. 28, no. 5, pp. 1007-1018, Oct. 2012.

[2] J.-S. Koh, S.-P. Jung, M. Noh, S.-W. Kim, and K.-J. Cho, "Flea Inspired Catapult Mechanism with Active Energy Storage and Release for Small Scale Jumping Robot," in *Proc. IEEE International Conference on Robotics and Automation*, 2013, pp. 26-31.

[3] J. Koh, S. Jung, R. J. Wood, and K.-J. Cho, "A jumping robotic insect based on a torque reversal catapult mechanism," in *Intelligent Robots and Systems (IROS), 2013 IEEE/RSJ International Conference on*, 2013, pp. 3796–3801.

[4] F. Li, G. Bonsignori, U. Scarfogliero, D. Chen, C. Stefanini, W. Liu, P. Dario, and X. Fu, "Jumping mini-robot with bio-inspired legs," in *Proc. IEEE International Conference on Robotics and Biomimetics*, 2008, pp. 933-938.

[5] M. Kovač, M. Fuchs, A. Guignard, J.-C. Zufferey, and D. Floreano, "A miniature 7g jumping robot," in *Proc. IEEE International Conference on Robotics and Automation*, 2008, pp. 373-378.

[6] R. Armour, K. Paskins, A. Bowyer, J. Vincent, and W. Megill, "Jumping robots: A biomimetic solution to locomotion across rough terrain," *Bioinspiration and Biomimetics*, vol. 2, no. 3, pp. S65-S82, 2007.

[7] B. G. A. Lambrecht, A. D. Horchler, and R. D. Quinn, "A small, insect-inspired robot that runs and jumps," in *Proc. IEEE International Conference on Robotics and Automation*, 2005, pp. 1240-1245.

[8] A. Yamada, M. Watari, H. Mochiyama, and H. Fujimoto, "An asymmetric robotic catapult based on the closed elastica for jumping robot," in *Proc. IEEE International Conference on Robotics and Automation*, 2008, pp. 232-237.

[9] J. Zhao, J. Xu, B. Gao, N. Xi, F. J. Cintron, M. W. Mutka, and L. Xiao, "MSU Jumper: A Single-Motor-Actuated Miniature Steerable Jumping Robot," *IEEE Transactions on Robotics*, vol. 29, no. 3, pp. 602–614, Jun. 2013.

[10] S. Bergbreiter and K. S. J. Pister, "Design of an autonomous jumping microrobot," in *Proc. IEEE International Conference on Robotics and Automation*, 2007, pp. 447-453

[11] W. A. Churaman, L. J. Currano, C. J. Morris, J. E. Rajkowski, and S. Bergbreiter, "The first launch of an autonomous thrust-driven microrobot using nanoporous energetic silicon," *Microelectromechanical Systems, Journal of*, vol. 21, no. 1, pp. 198–205, 2012.

[12] R. M. Alexander, *Principles of Animal Locomotion*. Princeton University Press, 2003.

[13] L. L. Howell, *Compliant mechanisms*. Wiley-Interscience, 2001.

[14] P. Fiorini and J. Burdick, "The development of hopping capabilities for small robots," *Auton. Robots*, vol. 14, no. 2–3, pp. 239–254, 2003.

[15] J. S. Kim, D. Y. Lee, J. S. Koh, G. P. Jung, and K.-J. Cho, "Component assembly with shape memory polymer fastener for microrobots," *Smart Materials and Structures*, vol. 23, no. 1, p. 015011, 2014.

[16] J. Kim, G. Jung, J. Koh, and K.-J. Cho, "Meso-scale robot assembly using shape memory polymer rivet fastener," in *Intelligent Robots and Systems (IROS), IEEE/RSJ International Conference on*, 2013, pp. 2082–2082.